

Performance studies of Time-of-Flight detectors at LHC

K. Černý¹, M. Taševský², T. Sýkora³, and R. Žlebčík³

¹*Regional Centre of Advanced Technologies and Materials, Joint Laboratory of Optics of Palacký University and Institute of Physics AS CR, Faculty of Science, Palacký University, 17. listopadu 12, 771 46 Olomouc, Czech Republic*

²*Institute of Physics of the Czech Academy of Sciences, Na Slovance 1999/2, 182 21 Prague 8, Czech Republic*

³*Institute of Particle and Nuclear Physics Faculty of Mathematics and Physics, Charles University, V Holešovičkách 2, 180 00 Prague 8, Czech Republic*

March 2, 2022

Abstract

We present results of a toy model study of performance of the Time-of-Flight detectors integrated into forward proton detectors. The goal of the ToF device is to suppress effects of additional soft processes (so called pile-up) accompanying the hard-scale central diffractive event, characterized by two tagged leading protons, one on each side from the interaction point. The method of mitigation of the pile-up effects exemplified in this study is based on measuring a difference between arrival times of these leading protons at the forward proton detectors and hence estimate the z-coordinate of the production vertex. We evaluate effects of the pile-up background by studying in detail its components, and estimate the performance of the ToF method as a function of the time and spatial resolution of the ToF device and of the number of pile-up interactions per bunch crossing. We also propose a new observable with a potential to efficiently separate central diffractive signal from the harsh pile-up environment.

1 Introduction

In diffractive processes, the leading protons produced with high rapidities carry a large fraction of the initial-state beam proton momentum and are separated from the rest of the hadronic final state by the so called large rapidity gap (LRG), i.e. non-exponentially suppressed rapidity interval devoid of particle activity introduced in [1] elaborated in [2]. Such a behaviour can be described by an exchange of a colorless strong state carrying quantum numbers of vacuum (so-called Pomeron) [3].

The diffractive processes in pp collisions at high energies can be divided into several categories according to the topology of the final state, see e.g. ref. [4]. We distinguish between the elastic processes (EL), single-diffractive dissociation (SD), double-diffractive dissociation (DD) and central-diffractive processes (CD). Should hard scales be present (represented by large masses or large transverse momenta in the final state) we speak of hard diffractive processes. The diagrams in figure 1 summarise topologies of the above-defined processes showing also the case of non-diffractive (ND) interactions.

In this text we focus on the CD processes, $pp \rightarrow pXp$, which represents the signal process, while the other topologies represent backgrounds. The experimental signature

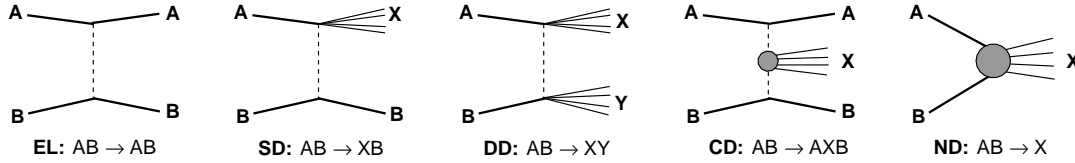


Figure 1: The main topologies of processes contributing to the total hadron-hadron cross section; elastic (EL), single-diffractive dissociation (SD), double-diffractive dissociation (DD), central-diffractive (CD) and non-diffractive processes (ND).

of CD events is characterized by a combination of measurement of the X system in the central detector and the detection of leading protons in the forward proton detectors (FPD) on both sides from the interaction point, referred to as A and B side in the positive and negative direction, respectively, of the interaction axis. The selection based on such a clear signature becomes less effective if there are more concurrent interactions taking place. This is typically the case at the LHC [5], where particle beams organised in particle bunches collide with high instantaneous luminosities. The mean number of collisions per single bunch crossing, $\langle\mu\rangle$ (also referred to as the pile-up), reached values of about 50 at LHC in 2018 [6] and is expected to be even higher at higher luminosity LHC phases [7].

In this study, we consider two ways the pile-up interactions can mimic the CD signal: in the first the X system of a non-CD process is reckoned as the signal in the central detector and leading protons from soft diffractive (SD or CD) processes are detected in FPDs, in the other the detected central system X and one of the leading protons come from a genuine CD process, while the other leading proton detected in FPD comes from a soft SD or CD process again.

As shown for the first time in ref. [8], the CD signal can effectively be separated from the pile-up effects described above by measuring arrival times of both leading protons to FPDs, equipped by Time-of-Flight (ToF) sub-detectors. In the following, we call this approach the ToF method. The ToF detectors can be integrated into FPDs as done in the AFP project [9] in the ATLAS experiment [10] or CT-PPS project [11] in the CMS [12] and TOTEM [13] experiments at the LHC. The difference between the arrival times of the two leading protons produced in the CD interaction (emitted in the opposite directions) is related to the z -position of their production vertex in the central detector, z_{PV} .

It is then evident that by requiring the z -positions of the vertex measured by the central detector and by FPDs to match within respective resolutions, the CD event can be separated from the pile-up backgrounds, as documented e.g. in refs. [14, 15, 16, 17, 18, 19]. The efficiency of this separation or the performance of the ToF method depends on number of parameters.

The primary one is the time resolution of the ToF detector. The other one is the amount of pile-up interactions in the central detector and consequently the number of leading protons produced in one bunch crossing. And the last one is the capability of the ToF detector to distinguish them, i.e. the spatial resolution or granularity of the ToF detector. Since it is not straightforward to calculate the impact of such effects analytically, we developed a model which we describe in the following.

2 Model of a single bunch crossing

The model described in this section simulates the features relevant to the measurement of central-diffractive processes using the ToF detectors in collisions of proton bunches at high instantaneous luminosity, i.e. in presence of pile-up interactions. Although the model is used to simulate effects at high $\langle\mu\rangle$ values (up to $\langle\mu\rangle \sim 200$), we do not make use of any additional information from timing detectors in the central detector as planned for ATLAS in ref. [20] and CMS in ref. [21] which would naturally lead to improvements in suppressing pile-up backgrounds.

2.1 Basic features of the model

For each bunch crossing, the model generates a number of vertices according to the Poisson distribution with mean value of $\langle\mu\rangle$. The vertices are generated in the z -coordinate (which is the beam collision axis) and time. Both quantities are randomly distributed according to a Gaussian distribution centred at zero and using the width stemming from the typical LHC luminous beamspot width in the z -coordinate (σ_{BS} and σ_{BS}/c for the spatial and time spreads, respectively). The bunch dimensions in the transverse directions as well as crossing angles of the beams are believed to have negligible impacts on the ToF evaluation and are, therefore, not simulated.

A special attention is paid to the choice of the primary vertex type. It is assumed that event observables seen by the central detector are reconstructed with respect to the primary vertex. For each event the model generates first one primary vertex of the desired type (CD, ND, SD or DD) and then adds further vertices from pile-up whose types are assigned with a probability proportional to their respective cross sections evaluated using PYTHIA 8 [22] at $\sqrt{s} = 13$ TeV. Therefore, there are four samples of events generated by the model denoted as CDPV, NDPV, SDPV and DDPV, depending on the process type assigned to the primary vertex. The EL processes are not expected to contribute, since they do not produce protons capable of reaching the FPDs.

The CD and SD vertices are further complemented by the leading proton(s) whose kinematics are taken from Pythia event files generated beforehand. The leading protons are subjected to a transport procedure mapping their momentum space kinematics to an auxiliary coordinate space (defined on the A and B sides) by means of which each leading proton is translated to a hit in the ToF detector. The hits are therefore defined by their local positions and times, where the time is defined by the production vertex time advanced or retarded proportionally to the vertex z -position and smeared using a Gaussian function with a width σ_t (ToF detector time resolution) on a random basis. On top of that an auxiliary detector is assumed to feature a spatial resolution parameter σ_x which can also be reckoned as a granularity parameter and serves to assess the impact of multi-hit events in the detector.

The initial setting of the beamspot size (50 mm), the size (2 cm) and location (1 mm from the nominal beam) of the detector as well as of the transport mapping (approximately linear in ξ) are chosen such that they do not depart too much from the realistic values available at the LHC. The main degrees of freedom of the model can thus be summarised as being represented by the values of $\langle\mu\rangle$, σ_{BS} , σ_t and σ_x . An additional freedom of the model is also introduced by the choice of the ToF detector positions and the transport details as well as by the methods used for dealing with multi-hit signals in the ToF detectors. It is also assumed that each arm is synchronized with the reference clock at a level of 2 ps (see Section 4.6.5.2 of ref. [9]).

Due to conservation laws the kinematics of the leading protons and the centrally pro-

duced system X of the primary CD process ($pp \rightarrow pXp$) are correlated. Strong correlations (even perfect within detector resolutions) are expected for exclusive processes, where the energy losses of the leading protons are fully transferred to the system X . In the case of inclusive CD processes, proton energy losses are shared between the system X and Pomeron remnants which usually continue in the direction of the incoming proton thus leave the central detector partly undetected. This leads to correlations which are significantly worse than in the case of exclusive processes. The correlations (or the lack of them) also allow for a better (or worse) separation of the genuine CD process from the non-CD ones. Because there are various processes that can be studied each with the specific experimental signature (topology of the X), dedicated cuts must always be applied to suppress various backgrounds including effects of pile-up. Any detailed analysis of the X topology and of the optimal cuts goes beyond the scope of the presented toy model. The model studies the kinematics and time information of the leading protons only.

2.2 Kinematics of signal events

The leading protons produced in the diffractive processes can be described in terms of the relative momentum loss (ξ), the Mandelstam (t) variable and the azimuthal angle (ϕ) (not considered here, usually integrated over), defined as

$$\xi = \frac{E_{\text{beam}} - E_p}{E_{\text{beam}}}, \quad (1)$$

$$t = (P_{\text{beam}} - P_p)^2, \quad (2)$$

where E_p (E_{beam}) represents the energy component of the leading (beam) proton four-vector, i.e. P_{beam} (P_p). The role of the t variable is negligible in the model. The most important is the energy of the beam proton available for the central interaction, i.e. ξE_{beam} .

In the case of the $pp \rightarrow pXp$ interactions the invariant mass and rapidity of the X system can be unambiguously related to the ξ fractions of the two leading protons as

$$m_X = \sqrt{s \xi_A \xi_B} \quad \text{and} \quad y_X = \frac{1}{2} \ln \left(\frac{\xi_A}{\xi_B} \right), \quad (3)$$

$$\xi_A = \frac{m_X e^{y_X}}{\sqrt{s}} \quad \text{and} \quad \xi_B = \frac{m_X e^{-y_X}}{\sqrt{s}}. \quad (4)$$

Of course, the above relations hold in case the X system is well resolved in the central detector which favours the exclusive processes in practice.

The m_X and y_X observables define the kinematic plane of CD processes. For a fixed value of one of the ξ fractions the y_X variable is a linear function of logarithm of m_X which simplifies the interpretation of the (m_X, y_X) kinematic plane. The range of kinematics where both leading protons end up in the acceptance of both ToF detectors, the so-called double-tag (DTAG) range, is very well defined then. A single variable (called d_{uv} here) can be constructed to assess the proximity of the CD event kinematics to the DTAG range, where the DTAG range is governed by the position and size of the ToF detectors. The definition of the d_{uv} discriminator is given in appendix A.

In figure 2a) the generated kinematics (m_X, y_X) of the primary CD processes in the CDPV sample is plotted for events with $\langle \mu \rangle = 10$ tagged on both sides (in detectors of 2 cm size placed 1 mm from the nominal position discussed with the transport in the next section). The DTAG range (indicated by the blue line) is visibly well enhanced as

the intersection of two strips that correspond to events with one leading proton tagged (single-tag, STAG).

The effect of pile-up interactions is visualized by shaded areas outside the STAG and DTAG areas.

As mentioned above, kinematics of the final state X system are not primarily analysed in the model. However, for the CD processes it makes sense to assume that the reconstruction of X would lead to values of m_X and y_X smeared by experimental resolutions of the central detector around the generated values which can be obtained via leading proton kinematics. Conservative resolutions of 30% and 0.3 for the reconstruction of m_X and y_X , respectively, are propagated to the d_{uv} calculation, thus corresponding to d_{uv}^{smeared} (or d_{uv}^{sm} for brevity). The functionality of the d_{uv} selection is evidenced by the b) and c) panels of figure 2.

In figure 2b) we document that the kinematics of the CDPV sample events, selected by the cut $d_{uv}^{\text{smeared}} = 1$, are constrained to a proximity of the DTAG range. Complementarily, in figure 2c) it is shown how relatively little of the generated kinematics leak outside the DTAG range due to smearing, if a $d_{uv}^{\text{gen}} = 1$ selection is applied.

Eventually, the distribution of the d_{uv}^{smeared} variable and its d_{uv}^{gen} components are shown in figure 2d). The d_{uv} discriminator clearly has a potential to suppress the contribution of CD events generated outside the DTAG acceptance which are falsely tagged due to the contribution of leading protons from pile-up. It represents an alternative approach to cuts realised as simple matching cuts between the m_X and y_X quantities measured in the central detector and the FPDs. The adequate value of the d_{uv}^{smeared} cut would be a matter of optimisation (not done here) depending on the actual precision of the m_X and y_X measurements.

2.3 The leading proton transport

The leading proton kinematics given in terms of ξ , t and ϕ affects the probability of detection of leading protons in FPDs. We use a simple transport linear in ξ disregarding the role of t and ϕ , implemented analytically as a $\xi \rightarrow x$ mapping defined as follows

$$x = 100 \xi [\text{mm}], \quad (5)$$

where the x value represents a hit position measured in the ToF detector.

The detectors are defined as sensitive volumes measuring the x -coordinate in an auxiliary x -space, where the $x = 0$ point represents the nominal beam. The detectors are given a length of 20 mm with the detector edge placed at $x = 1$ mm from the origin of coordinates as a baseline position, which limits the measurable ξ values to the range of 0.01–0.21.

The detector dimensions, position and the resulting range of accessible ξ values are similar to those usually achievable by FPDs for hard diffractive physics at LHC experiments. Possible non-linearities and smearings of the mapping (due to the limited position resolution, beamspot smearing and folding of the t and ϕ kinematics) are neglected here. The mapping is for example useful to study the impact of limited granularity which is realised here as an equidistant division of the sensitive detector range to cells of the σ_x size.

2.4 Analysis of generated events

The generated event data contain information about the primary vertex z -position, z_{PV} , and positions and times of hits measured in the two FPDs. A hit filtering procedure is

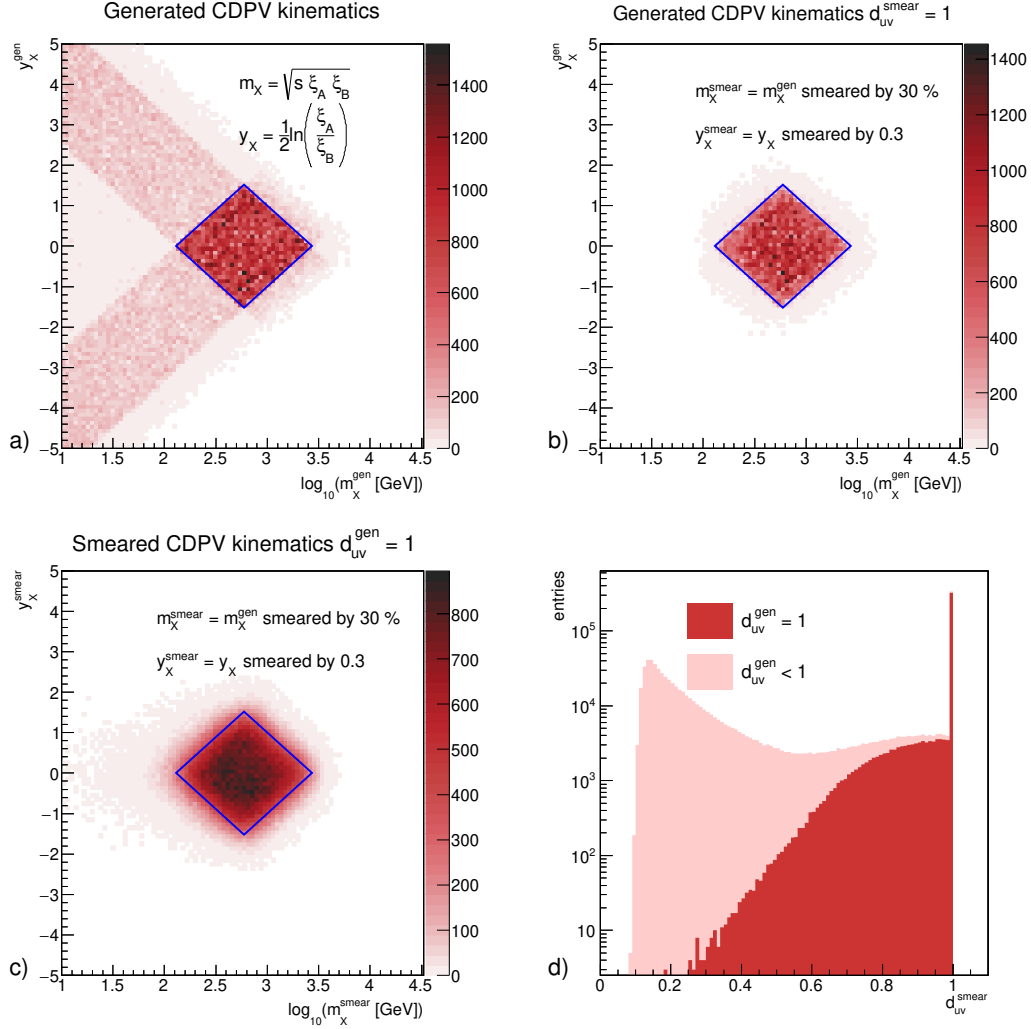


Figure 2: Generated and smeared kinematics of central diffractive processes in the CDPV sample overlaid with pile-up ($\langle \mu \rangle = 10$) with signal in the detectors of 2 cm size located 1 mm from the nominal beam. The smearing of generated values is done using resolutions of 30% for the m_X and 0.3 for the y_X variable. a) Generated CD kinematics together with the DTAG range indicated by the blue line, b) effect of the $d_{\text{uv}}^{\text{smeared}}$ cut on generated kinematics, c) smeared kinematics selected by the $d_{\text{uv}}^{\text{gen}}$ cut, d) distribution of the $d_{\text{uv}}^{\text{smeared}}$ discriminant obtained from the smeared generated kinematics. The contribution of CD events with true kinematics generated in the DTAG range is emphasised by the dark red histogram, the events outside the true DTAG range are represented by the pale red histogram.

adopted such that hits occupying the same detector cell are merged into one new hit with a time stamp of the earliest one.

The case of $\sigma_x = 0$ is a special case of a detector with an ideal granularity, i.e. no hit filtering.

For each particular pair of hits from opposite sides, the z_{ToF} variable can be reconstructed as

$$z_{\text{ToF}} = -\frac{c}{2}(t_A - t_B), \quad (6)$$

We assume that FPDs at the A and the B sides are located at the same distances from the interaction point. If there are multiple pairs of hits, a list of z_{ToF} vertices is obtained.

On the event-by-event basis, each of the list of z_{ToF} vertices is compared with the value of z_{PV} thereby forming a $\Delta z = z_{\text{PV}} - z_{\text{ToF}}$ distribution. While the width of the Δz distribution in the signal CDPV sample is proportional to $c\sigma_t$, the widths in the background samples are much broader and depend on σ_{BS} . More precisely, the width of the signal Δz distributions neglecting the primary vertex reconstruction uncertainty is given by $c\sigma_t/\sqrt{2}$ which is used as the cut applied to select the genuine CD events (so called Δz veto), i.e.

$$|\Delta z| < \frac{c}{\sqrt{2}}\sigma_t. \quad (7)$$

There are two kinds of background contributions to the Δz distribution. The first one originates from independent combinations of the $(z_{\text{ToF}}, z_{\text{PV}})$ values, where z_{ToF} is reconstructed from hits generated by pile-up interactions only. A single Gaussian shape of such contribution is expected with a width of $\sqrt{2}\sigma_{\text{BS}}$ ¹. The second kind of background (partially tagged) can be expected to contribute in the CDPV sample only, where one of the hits used for the z_{ToF} calculation was caused by a genuine leading proton generated in the CD event in the primary vertex. The width of this partially tagged background is equal to σ_{BS} . The Δz widths of all considered backgrounds are discussed in detail in the appendix B.

It is convenient to use space-time coordinates to depict the rationale behind the ToF method as demonstrated in figure 3, where topologies of signal and different backgrounds are shown (the space-time coordinates are scaled to equal display units). The Gaussian bunch-crossing contours of width σ_{BS} are indicated by the shaded circle. The leading protons are indicated by $\pm 45^\circ$ lines reaching positions of FPD detectors on sides A and B. In figure 3a) the simplest CD process from the CDPV sample is visualized where both detectors provide information consistent with the primary vertex position within the σ_t range shown by dashed lines along the leading proton nominal lines. In figure 3b) the pile-up background in the CDPV cases is sketched, which produces the identical background shape as the non-CDPV samples, i.e. NDPV in figure 3d) for instance. This is caused by the fact that the fake (having in mind the spurious vertices reconstructed from SD events) and possibly also the non-primary CD vertices are distributed independently of z_{PV} , both with σ_{BS} widths. The origin of the partially tagged CDPV background is also shown in figure 3c) where the main ingredient is the fact that one of the measured proton arrival times is coming from the actual CD-primary vertex. In order to form pairs, pairs of hits from opposite sides are formed which leads to reconstruction of fake vertices that are no longer distributed independently in space and time, they populate a (z, t) world-line defined by the tagged proton from the primary CD process.

The points discussed above are illustrated in the plot in figure 4a), where the Δz distributions are plotted for CDPV and NDPV samples for $\langle \mu \rangle = 10$, $\sigma_t = 30$ ps and

¹if σ_t is neglected

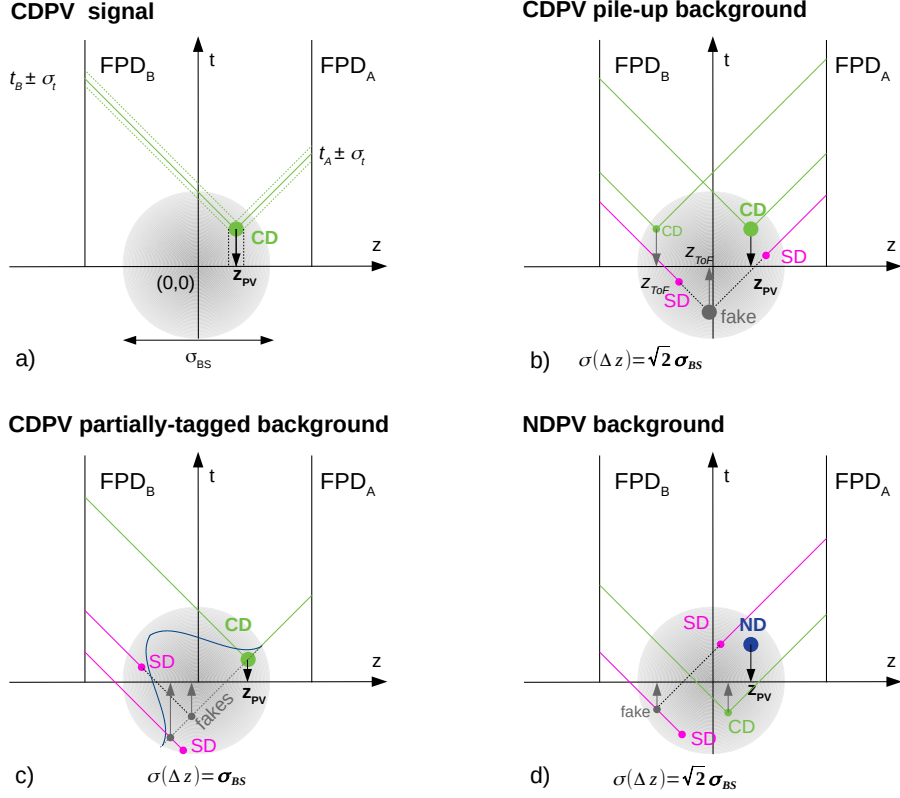


Figure 3: The space-time diagrams describing the rationale behind the use of Time-of-Flight method. The horizontal and vertical axes correspond to the z -coordinate and time, respectively, where the centre of the beam spot (represented by the large shaded circle) is located in the origin of coordinates. The positions of the time-measuring FPD detectors are indicated by the vertical lines at fixed z positions. The world lines of the leading protons travelling at speed of light are sketched with $\pm 45^\circ$ lines and primary vertices are represented by circles (green for CD, magenta for SD and blue for ND processes) and marked by z_{PV} . The vertices coming from ToF measurements and marked by z_{ToF} (represented by small grey circles) are caused by a fake double-tag of two leading protons from two unrelated events and are put at the intersection of corresponding lines going in opposite directions.

$\sigma_x = 0$. The signal and background contributions to the total Δz distribution in the CDPV sample are shown where the fractional partial-tag CDPV background is indicated and fitted separately. The fitted widths of the signal (6.4 mm) and background distributions (50.3 mm and 70.8 mm²) are consistent with the input values of $\sigma_t = 30$ ps and $\sigma_{BS} = 50$ mm. In the NDPV sample the Δz variable contains only one background component described by a single Gaussian fit of a 70.9 mm width as expected. In figure 4b) results for the same components to the total Δz distribution are shown for an alternative definition of the Δz variable, namely only a single Δz value closest to the z_{PV} is considered per event, denoted as Δz_{min} . The shapes of the signal and background components are not Gaussian and no attempt to perform fits was made. The advantage of this method is that one has just one value of $\Delta z = \Delta z_{min}$ per event to deal with.

²where $50\sqrt{2} \simeq 70.7$

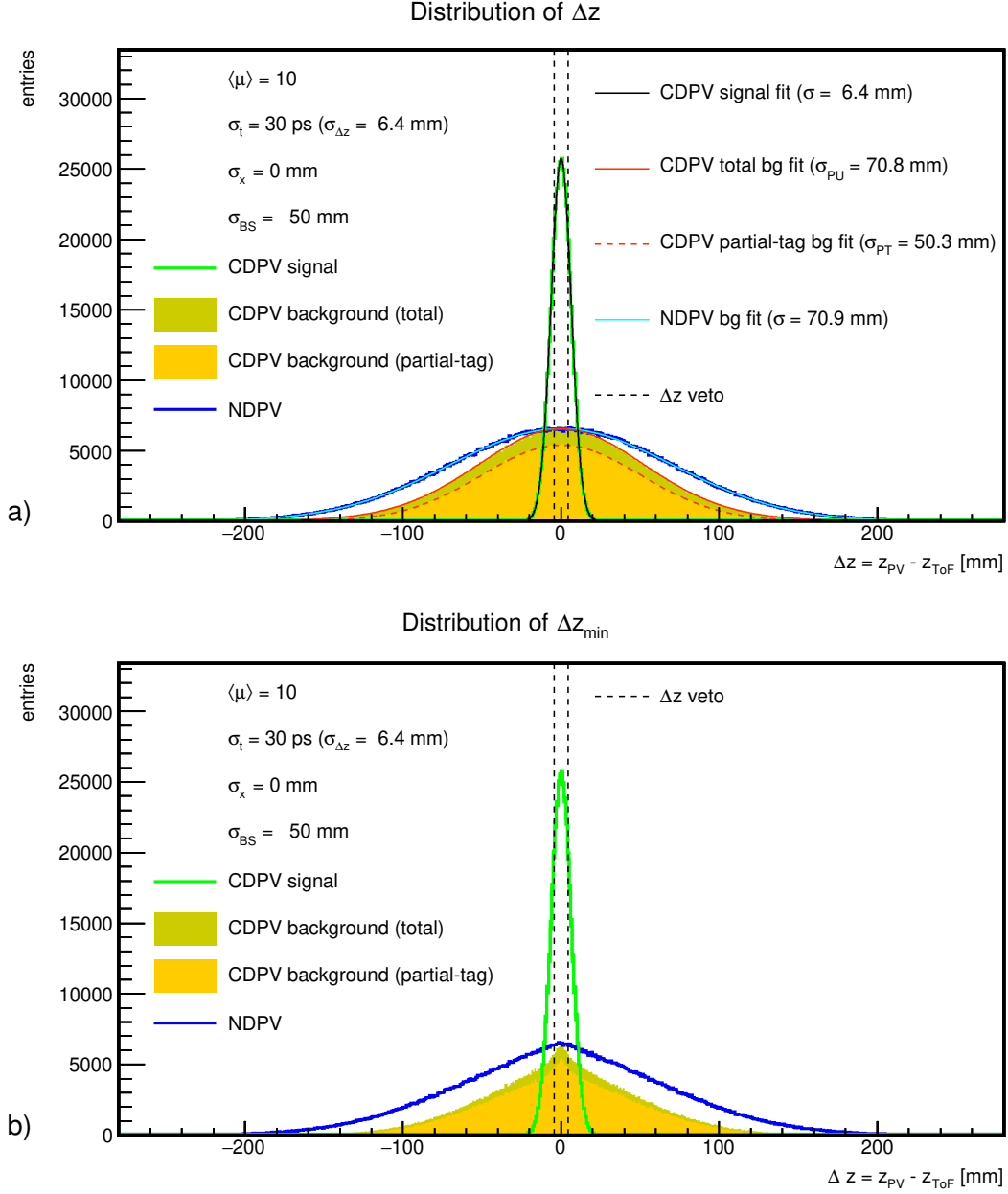


Figure 4: Unnormalized Δz distributions in the CDPV and NDPV samples generated using $\langle \mu \rangle = 10$, $\sigma_t = 30$ ps, $\sigma_x = 0$ and $z_{BS} = 50$ mm. a) The signal is shown by the light green histogram and total CDPV, partially-tagged CDPV and NDPV backgrounds by the dark yellow, yellow and blue histograms, respectively. Fits to the distributions are shown by lines. The fitted widths of the CDPV background components are denoted as σ_{PU} and σ_{PT} for the pile-up and partial-tag contributions. The Δz veto is indicated by the vertical dashed black lines. b) The same distributions are shown for the Δz_{min} method with the same color coding as in a).

3 Results

In this section we discuss results obtained from the toy model and the performance of the ToF method to extract the CD signal from pile-up backgrounds only on the basis of kinematics of forward protons detected in ToF detectors. We assume that the primary selection of a CD process under study in an offline analysis would be based on a central-detector trigger part followed by a proper analysis of the hadronic final state X .

In the following analysis the events with ND and SD processes in the primary vertex are assumed to represent backgrounds and to contaminate the sample of selected events. The contribution of the DD background ($pp \rightarrow XY$) process is neglected thanks to a very different final state comprising two forward-going systems X and Y , separated by a large rapidity gap, and missing leading protons produced directly. The EL processes are naturally neglected as well because they do not mimic neither the central system X , nor the leading protons.

The probability of the signal observation in the two ToF detectors in a single event represents a first observable measured by the model. It is defined as

$$P_{\text{DTAG}} = \frac{N_{\text{DTAG}}}{N_{\text{gen}}}, \quad (8)$$

where N_{gen} is the number of events needed to obtain N_{DTAG} events that satisfy the DTAG condition.

For the latter then the probability that a given event is selected by having at least one entry in the Δz window, i.e. passing the Δz veto (eq. (7)), is calculated as

$$P_{\Delta z} = \frac{N_{\Delta z\text{-cut}}}{N_{\text{DTAG}}}, \quad (9)$$

where $N_{\Delta z\text{-cut}}$ denotes the number of events with at least one entry in the Δz window, i.e. involving signal or pile-up protons. Finally, the probability that the Δz veto is satisfied through detection of the primary CD process is denoted by $P_{\Delta z}^{\text{signal}}$. The $P_{\Delta z}^{\text{signal}}$ quantity is therefore only defined on the CD signal events from the CDPV sample, i.e. those having two genuine leading protons originating in the primary vertex and not from accompanying pile-up events.

The P_{DTAG} and $P_{\Delta z}$ are also calculated for the case when the events of the CDPV sample are preselected by the d_{uv} cut. Since this cut selects events with kinematics close to the DTAG range, P_{DTAG} and $P_{\Delta z}$ values are naturally enhanced.

In figure 5a) the probability of observing events tagged by ToF detectors on both sides, P_{DTAG} , is shown as a function of $\langle\mu\rangle$ in the form of colored bands for CDPV (green), NDPV (blue) and SDPV (magenta) samples. Each band represents an envelope of studied edge positions $x_{\text{min}}^{\text{det}}$. Top lines correspond to 1 mm, center lines to 1.5 mm and bottom lines to 2 mm and differences with respect to the central values are within 10%. The effect of using the d_{uv} discriminator cut (realised as $d_{\text{uv}}^{\text{smear}} = 1$) on signal CDPV events is clearly demonstrated by the orange band, to be compared with the green one, corresponding to only the DTAG condition used with no other constraints. Differences between green, magenta and blue bands are easily explained by the fact while the number of pile-up vertices is the same for all samples for a given value of $\langle\mu\rangle$, the number of leading protons is smallest for the NDPV sample and is greater by one for the SDPV and by two for the CDPV sample. That is why the P_{DTAG} differences diminish with increasing $\langle\mu\rangle$. Finally, we note that the P_{DTAG} values were observed to be insensitive to the time resolution or the hit merging caused by a limited granularity.

The P_{DTAG} values resulting from our model and their $\langle\mu\rangle$ -dependence can be compared with literature. A combinatorial formula was for instance derived in ref. [16] (see eq. (1) there). As seen in figure 5b), the averaged P_{DTAG} probabilities obtained from the toy model as a weighted sum using respective cross-sections of the ND, SD and CD processes, whose sum is denoted as minimum bias (MB), are found consistent with the prediction of the published combinatorial formula for $x_{\text{min}}^{\text{det}} = 1.5$ mm. The input parameter to the combinatorial formula is the probability of single-tagging, A_{ss} . In our case A_{ss} is evaluated as

$$A_{ss} = \frac{\sigma_{\text{SD}}A_{\text{SD}} + \sigma_{\text{CD}}A_{\text{CD}}}{\sigma_{\text{inel}}}, \quad (10)$$

where the factors 'A' denote the acceptance of FPDs for each process capable of producing leading protons, i.e. fraction of events with ξ values inside the detector acceptance. This in turn means that one can use the analytic prescription to get an idea on how further acceptance changes (e.g. caused by a limited detection efficiency of detectors) propagate to the result. A substitution of $\langle\mu\rangle$ by $\langle\mu\rangle - 1$ is used in the formula and corresponds to the fact that one of the vertices is already occupied by the primary vertex (of a hard-scale event) in the toy model.

In figures 6a), 7a) and 8a) the $P_{\Delta z}$ probabilities are shown for the same PV samples and d_{uv} cut used as in figure 5, now for three granularity choices of 0, 2 and 5 mm in each figure and three timing resolutions of 10, 20 and 30 ps, respectively. Now the different granularities make a difference, the observed probabilities decrease with the granularity parameter σ_x increasing. The probabilities for CDPV events start at $\sim 68\%$ and evolve slowly with $\langle\mu\rangle$ for the d_{uv} selected events. The changes in $P_{\Delta z}$ introduced by changes of granularity do not seem to be dramatic for the event yields. The $P_{\Delta z}$ values for the CDPV sample with d_{uv} selection relaxed decrease rapidly with $\langle\mu\rangle$ increasing approaching the trends of SDPV and NDPV samples. The fraction of background events passing the Δz cut increases with increasing $\langle\mu\rangle$.

In figures 6b), 7b) and 8b) the $P_{\Delta z}^{\text{signal}}$ values are shown for the CDPV samples for the granularity and ToF timing resolution as before. The results are presented for events with or without the d_{uv} cut and the Δz and Δz_{min} cut method. The decrease of $P_{\Delta z}^{\text{signal}}$ selected with d_{uv} cut for all granularities with Δz_{min} method is not surprising, since it only reflects the fact that occasionally the minimum value of Δz in the event can be produced by the pile up interaction. The effect is becoming more visible with timing resolution worsening, because the Δz window widens with σ_t . The observation of low $P_{\Delta z}^{\text{signal}}$ values for CDPV events selected using a relaxed d_{uv} cut supports the need for a well designed pre-selections of events by the central detector.

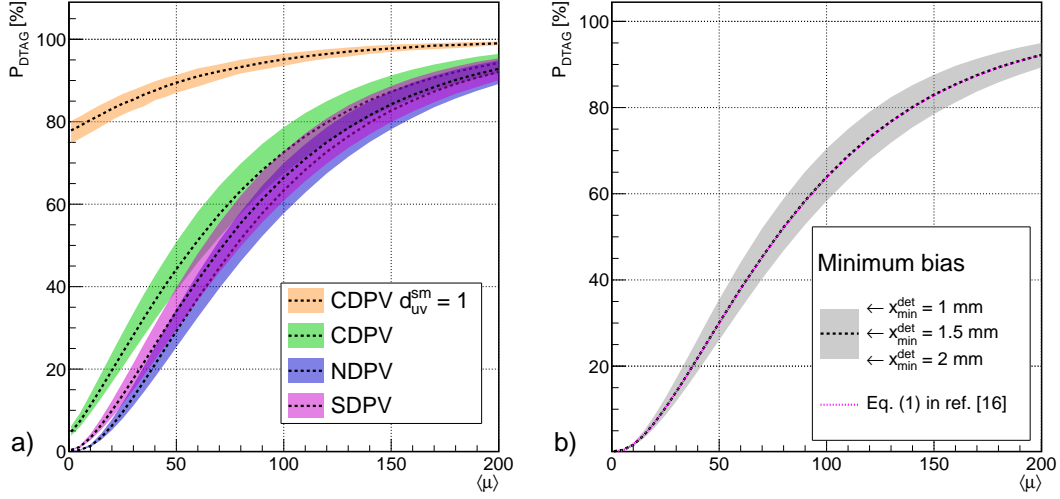


Figure 5: a) ToF double-tag probability as a function of $\langle\mu\rangle$ for three detector edge positions shown as coloured bands where values from the top (bottom) of the bands correspond to $x_{\text{min}}^{\text{det}} = 1$ (2) mm and the middle dashed lines indicate the $x_{\text{min}}^{\text{det}} = 1.5$ mm results. The green, magenta and blue bands represent results from the CDPV, SDPV and NDPV samples, respectively, the orange band shows results from the CDPV sample where the generated kinematics are constrained by $d_{\text{uv}}^{\text{smear}} = 1$. b) P_{DTAG} values obtained as weighted average of the CDPV, NDPV and SDPV values and represented by the white dashed line are compared with the prediction based on eq. (1) in ref. [16] shown by the magenta dotted line for the case of $x_{\text{min}}^{\text{det}} = 1.5$ mm.

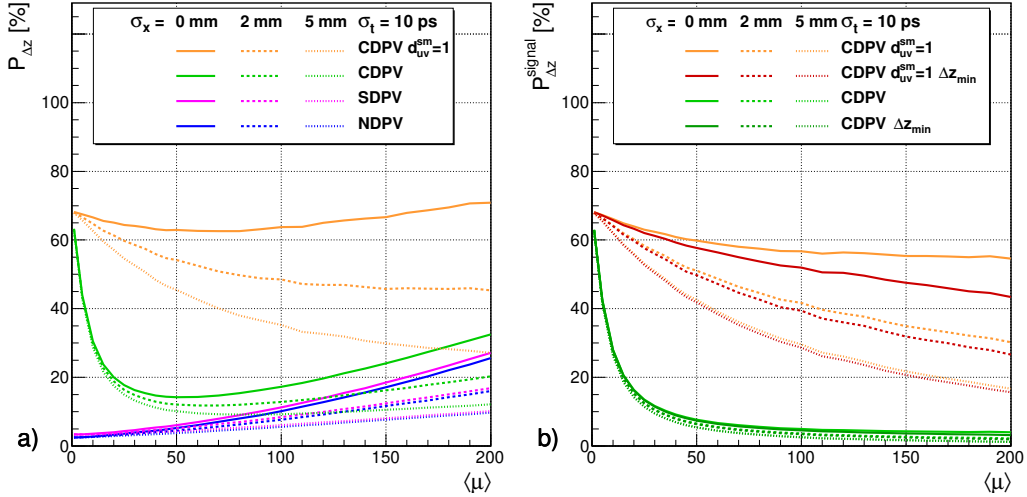


Figure 6: $P_{\Delta z}$ and $P_{\Delta z}^{\text{signal}}$ probabilities as a function of $\langle\mu\rangle$ for $\sigma_t = 10$ ps and three σ_x values of 0, 1 and 2 mm shown by solid, dashed and dotted lines. a) $P_{\Delta z}$ of the CDPV sample using the $d_{\text{uv}}^{\text{smear}} = 1$ selection are shown by the orange lines, the unconstrained case $P_{\Delta z}$ is shown in green. The NDPV and SDPV values are shown by blue and magenta lines. b) $P_{\Delta z}^{\text{signal}}$ results corresponding to the $d_{\text{uv}}^{\text{smear}} = 1$ selection using all measured Δz values are shown by the orange lines. The results for Δz_{min} method is shown by the dark red lines. $P_{\Delta z}^{\text{signal}}$ of the unconstrained case is shown by the green and dark green lines.

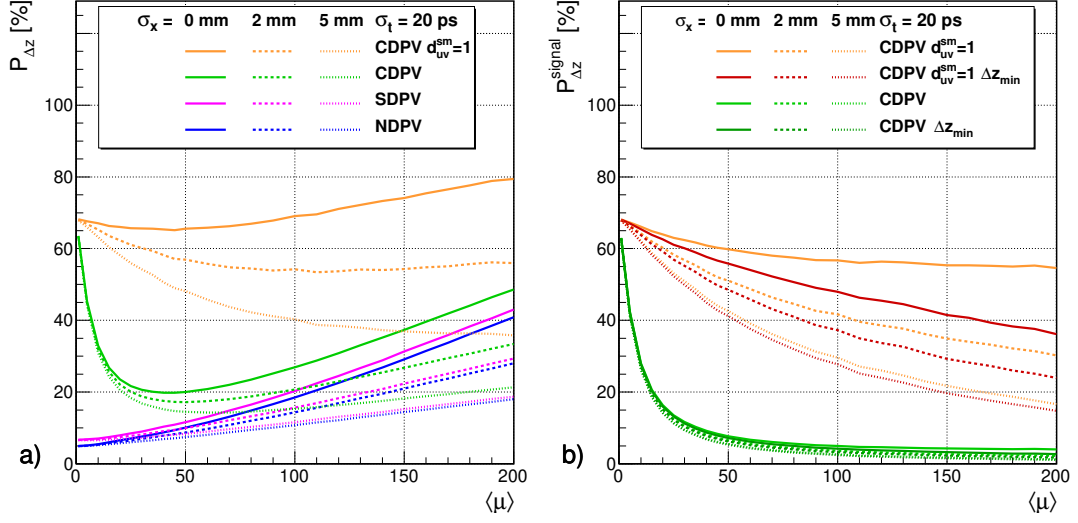


Figure 7: The $P_{\Delta z}$ and $P_{\Delta z}^{\text{signal}}$ presented in the same manner as in figure 6 for the timing resolution of 20 ps.

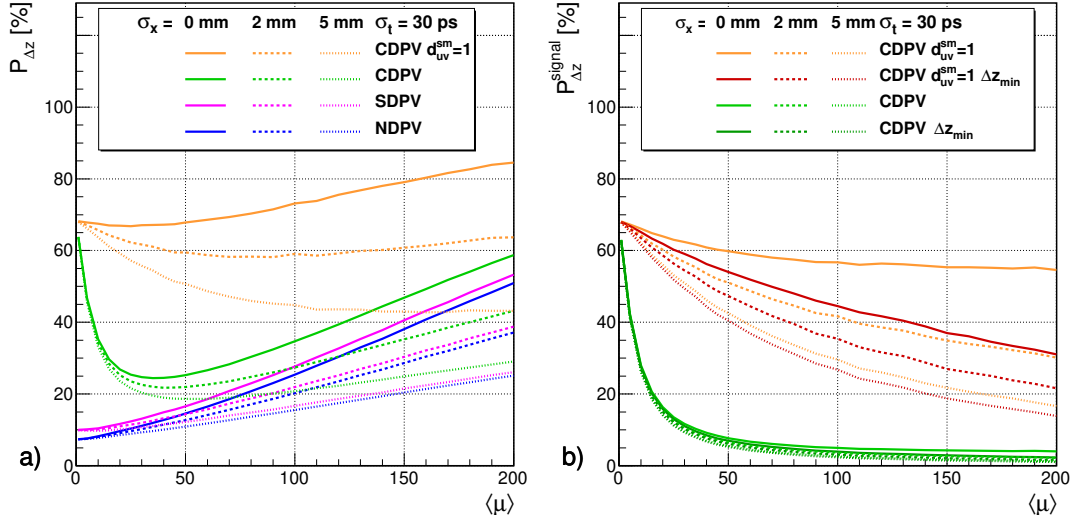


Figure 8: The $P_{\Delta z}$ and $P_{\Delta z}^{\text{signal}}$ presented in the same manner as in figure 6 for the timing resolution of 30 ps.

4 Conclusions

We have developed a simple model to study the performance of the Time-of-Flight detectors to efficiently separate central diffractive events from the harsh pile-up environment. The model works with basic assumptions on the transport of leading protons from the interaction point to forward proton detectors and on time and spatial resolutions of the ToF device. We have provided a generic double-tag probability for the signal and all relevant backgrounds stemming from pile-up interactions, as a function of the time and spatial resolutions of the ToF device and the amount of pile-up per bunch crossing, in the ranges

of σ_t of 10–30 ps, σ_x of 0–5 mm and $\langle\mu\rangle$ of up to 200. This double-tag probability is to be in an ideal case scaled by selection efficiencies for the signal or rejection efficiencies for backgrounds for each process under study.

The effect of the time resolution is observed to be rather negligible for the CD signal and more-or-less linearly increasing with increasing σ_t for pile-up backgrounds.

The effect of the granularity is in general more pronounced for the signal as well as backgrounds and, as expected, while it decreases for the signal, it increases for the backgrounds with increasing σ_x . For both these effects, it holds that as the amount of pile-up interactions grows, the effect gets stronger.

As to the shape of the $\Delta z = z_{\text{PV}} - z_{\text{ToF}}$ distribution, it was found that the background contribution has two components of different widths – which may be a useful information for the physics analysis of the real data.

We have studied two methods of the event selection using the Δz variable, the inclusive and minimum method. While the former is based on looping over all Δz values constructed from all combinations using the list of available z_{ToF} values, the latter uses only the z_{ToF} value closest to the primary vertex position. The advantage of the Δz_{min} method is a simpler implementation. Disadvantages are a non-trivial Δz shape and lower probabilities of signal detection in the case of unfavourable time resolutions and granularities of the ToF detectors.

The importance of coupling the ToF detector (or FPD) acceptance with the information from the central detector is demonstrated by the use of d_{uv} discriminator developed specifically for this study. The derivation of this discriminator is based on a set of generated kinematics (m_x and y_x) conveniently transformed to a single-valued observable. The smeared kinematics entering the d_{uv} calculation resulting in a cut on $d_{\text{uv}}^{\text{smeared}}$ enhance the fraction of signal events capable of reaching the ToF detectors. In a real data taking the kinematics of the signal are primarily constrained by the trigger followed by another set of cuts relating the central detector observables with those reconstructed from measurements of leading protons in FPDs. Here we only demonstrate that the probability of double-tagging for the central diffractive signal can significantly be enhanced by taking into account kinematical constraints from the central detector.

Acknowledgements

The authors gratefully acknowledge the support of the following projects: Karel Černý through CZ.02.1.01/0.0/0.0/16_019/0000754 of The Ministry of Education, Youth and Sports the Czech Republic (MEYS); Tomáš Sýkora through LM2015056 and LTT17018 of MEYS; Marek Taševský through LTT17018 of MEYS; Radek Žlebčík through Charles University Research Center (UNCE/SCI/013).

A Double tag discriminator

Here, a discriminator variable, d_{uv} , of the kinematics m_x, y_x generated inside or outside the double tag range is derived.

From equations (3) and (4) it can be seen that y_x depends linearly on logarithm of m_x for a fixed value of one of the ξ fractions. For a fixed ξ_B one can write

$$\begin{aligned}
y_X(m_X, \xi_B = \text{const}) &= \frac{1}{2} \ln \frac{\xi_A}{\xi_B} = \ln \frac{\sqrt{s\xi_A\xi_B}}{\sqrt{s\xi_B^2}} = \\
&= \ln m_X - \ln(\sqrt{s\xi_B}).
\end{aligned} \tag{11}$$

The formula (11) corresponds to a linear change of y_X with m_X with a positive slope. The negative slope dependence corresponds to a fixed ξ_A as

$$y_X(m_X, \xi_A = \text{const}) = -\ln m_X + \ln(\sqrt{s\xi_A}). \tag{12}$$

We can also note further symmetry properties defined by four major points in the (m_X, y_X) kinematic plane (for an idea about symmetries, see figure 2), i.e.

$$m_1 = \sqrt{s\xi_{\min}}, \quad y_1 = \frac{1}{2} \ln \frac{\xi_{\min}}{\xi_{\min}} = 0, \tag{13}$$

$$m_2 = \sqrt{s\xi_{\max}\xi_{\min}}, \quad y_2 = \frac{1}{2} \ln \frac{\xi_{\max}}{\xi_{\min}}, \tag{14}$$

$$m_3 = \sqrt{s\xi_{\max}}, \quad y_3 = \frac{1}{2} \ln \frac{\xi_{\max}}{\xi_{\max}} = 0, \tag{15}$$

$$m_4 = \sqrt{s\xi_{\min}\xi_{\max}}, \quad y_4 = \frac{1}{2} \ln \frac{\xi_{\min}}{\xi_{\max}}, \tag{16}$$

where the (m_1, y_1) point denotes the point of mass threshold of double tagging while the (m_3, y_3) indicates the point of maximum achievable mass. The (m_2, y_2) and (m_4, y_4) points represent the points of maximum and minimum rapidity, respectively, measurable in the double tagged case. If logarithm of a generic base, $\log m_X$, is used the $\log m_2$ and $\log m_4$ divide the $(\log m_1, \log m_3)$ interval in halves since

$$\begin{aligned}
\frac{1}{2} (\log m_1 + \log m_3) &= \frac{1}{2} (\log \sqrt{s\xi_{\min}} + \log \sqrt{s\xi_{\max}}) = \\
&= \frac{1}{2} \log s\xi_{\min}\xi_{\max} = \\
&= \log \sqrt{s\xi_{\min}\xi_{\max}} = \log m_2 = \log m_4.
\end{aligned} \tag{17}$$

The kinematics of the double tag events in the $\log m_X$ and $|y_X|$ is represented by a triangle using the $\pm y_X$ symmetry. If basis vectors defined by two line segments of the kinematic triangle are used (\vec{e}_u, \vec{e}_v) , parametric coordinates (u, v) define a new parametric triangle (uv -triangle), see figure 9. The points belonging to the triangle satisfy $u, v \in \langle 0, 1 \rangle$ and $u + v \leq 1$. The area of the uv -triangle is equal to 0.5. Any point inside a reference convex polygon satisfies the condition that the sum of areas of triangles defined by the sides of the polygon and the tested point equals the polygon area. Any point outside the tested polygon gives a sum larger than the area of the reference polygon. This condition is tested by the calculation of d_{uv} variable defined as

$$d_{uv} = \frac{0.5}{\sum_{i=1}^3 A_i}, \tag{18}$$

where the reference value of 0.5 refers to the uv -triangle area and the A_i sum term provides a handle on the general point position with respect to the triangle as indicated in figure 9.

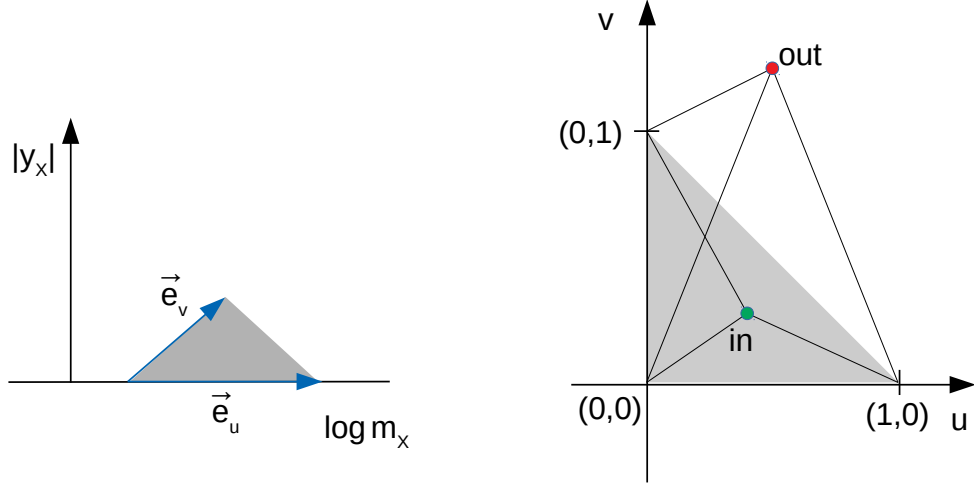


Figure 9: The parameterisation of kinematics of double tagged events in the $(\log m_X, |y_X|)$ plane (left) and in the (u, v) plane (right).

The parametric coordinates in terms of m_X and y_X are defined as follows

$$u = \frac{1}{\ln \frac{m_{X,\max}}{m_{X,\min}}} \left[\ln \left(\frac{m_X}{m_{X,\min}} \right) - |y_X| \right], \quad (19)$$

$$v = \frac{2|y_X|}{\ln \frac{m_{X,\max}}{m_{X,\min}}}, \quad (20)$$

where the absolute value of y_X indicates that we employ the $\pm y_X$ symmetry. The $m_{X,\max}$ and $m_{X,\min}$ correspond to m_1 and m_3 values defined in eqs. (13) and (15).

The $\sum_{i=1}^3 A_i$ term can eventually be written down as

$$\sum_{i=1}^3 A_i = \frac{1}{2} (|u| + |v| + |u + v - 1|), \quad (21)$$

leading to the following formula for d_{uv} :

$$d_{uv} = (|u| + |v| + |u + v - 1|)^{-1}. \quad (22)$$

B Bunch size propagation to the ToF measurements

Let us assume that the longitudinal relativistically contracted width of the Gauss-shaped particle bunch in the laboratory frame is $\sigma_z = c\sigma_T$, where σ_T is the corresponding 1- σ width in time³. The PDF representing the longitudinal distribution of the beam spot is

³The bunch width is often quoted in terms of $4\sigma_T$ at the LHC.

obtained as a convolution of the PDFs of two bunches moving in time, i.e.

$$\begin{aligned}
f(z) &= \int_{-\infty}^{+\infty} dt e^{-\frac{1}{2}\left(\frac{z-ct}{\sigma_z}\right)^2} e^{-\frac{1}{2}\left(\frac{z+ct}{\sigma_z}\right)^2} = \\
&= e^{-\frac{1}{2}\left(\frac{z}{\sigma_z/\sqrt{2}}\right)^2} \underbrace{\int_{-\infty}^{+\infty} dt e^{-\frac{1}{2}\left(\frac{ct}{\sigma_z/\sqrt{2}}\right)^2}}_{\text{constant}}.
\end{aligned} \tag{23}$$

This means that the width along the z -direction of the beam spot reads

$$\sigma_{\text{BS}} = \sigma_z / \sqrt{2}. \tag{24}$$

The z_{ToF} vertex position is inferred from the measurements of leading proton arrival times as $z_{\text{ToF}} = -\frac{c}{2}(t_A - t_B)$, where $t_{A(B)}$ represents the arrival time of the leading proton to the $A(B)$ -side detector. The positive (negative) z -side corresponds to the $A(B)$ -side. The arrival time is given by the production vertex time, t_{pr} , retarded (advanced) proportionally to the production vertex z -position, z_{pr} , as

$$t_{A(B)} = \frac{d}{c} - (+) \frac{z_{\text{pr}}}{c} + t_{\text{pr}}, \tag{25}$$

where the production vertex values are measured with respect to $t_{\text{pr}} = 0$ and $z_{\text{pr}} = 0$ and where equal distances d are assumed from $z_{\text{pr}} = 0$ to each of the detectors meaning that the distance becomes irrelevant for the z_{ToF} calculation.

The values, z_{pr} and ct_{pr} are distributed with the σ_{BS} width. From using the equation (25) it implies that the width of $ct_{A(B)}$ distributions equals $\sqrt{2}\sigma_{\text{BS}}$. The width of the z_{ToF} distribution (given by eq. (6)) obtained from independent production vertices reads

$$\sigma(z_{\text{ToF}})^{\text{indep.}} = \frac{1}{2} \sqrt{\text{Var}(z_{\text{pr}} - ct_{\text{pr}} + z'_{\text{pr}} + ct'_{\text{pr}})} = \frac{1}{2} \sqrt{4\sigma_{\text{BS}}^2} = \sigma_{\text{BS}}, \tag{26}$$

where the un-primed (primed) values correspond to the $A(B)$ -side which originate in different unrelated interactions. In the case of interactions leading to the production of two leading protons (central diffraction, CD) registered on both sides, a σ_{BS} width is expected of the z_{ToF} given by

$$\begin{aligned}
\sigma(z_{\text{ToF}})^{\text{CD}} &= \frac{1}{2} \sqrt{\text{Var}(z_{\text{pr}} - ct_{\text{pr}} + z_{\text{pr}} + ct_{\text{pr}})} = \\
&= \frac{1}{2} \sqrt{\text{Var}(2z_{\text{pr}})} = \frac{1}{2} \sqrt{4\sigma_{\text{BS}}^2} = \sigma_{\text{BS}}.
\end{aligned} \tag{27}$$

The distribution of the observable Δz defined as $\Delta z = z_{\text{PV}} - z_{\text{ToF}}$, where z_{PV} is the position of the primary interaction vertex, has two background contributions with different width depending on the type of z_{ToF} hypothesis considered. The width of the Δz distribution provided by the z_{ToF} values obtained from arrival times of unrelated interactions and z_{PV} positions of events independent of the ToF tagged ones, i.e. z_{PV} , t_A and t_B independent (called *untag* as no leading proton from the primary vertex contributes), is analogously to equation (26) given by

$$\begin{aligned}
\sigma(\Delta z)^{\text{untag}} &= \sqrt{\text{Var}\left(z_{\text{PV}} - \frac{z_{\text{pr}}}{2} + \frac{ct_{\text{pr}}}{2} - \frac{z'_{\text{pr}}}{2} - \frac{ct'_{\text{pr}}}{2}\right)} = \\
&= \sqrt{\sigma_{\text{BS}}^2 + 4\frac{\sigma_{\text{BS}}^2}{4}} = \sqrt{2}\sigma_{\text{BS}}.
\end{aligned} \tag{28}$$

The same Δz width of $\sqrt{2}\sigma_{\text{BS}}$ is expected in the fraction of z_{ToF} values where the arrival times of double tagged CD interactions are measured in events where the z_{PV} comes from an independent process, which can be seen from eq. (28) using eq. (27).

A special case as to the Δz width arises when one of the arrival times is actually provided by leading proton originating in the primary interaction process taking place at z_{PV} and an unknown time t_{PV} (denoted as *partial-tag*). With no loss of generality let us assume the A-side values to equal $t_{\text{pr}} = t_{\text{PV}}$ and $z_{\text{pr}} = z_{\text{PV}}$ in equation (28) leading to

$$\begin{aligned}\sigma(\Delta z)^{\text{partial-tag}} &= \sqrt{\text{Var}\left(z_{\text{PV}} - \frac{z_{\text{PV}}}{2} + \frac{ct_{\text{PV}}}{2} - \frac{z'_{\text{pr}}}{2} - \frac{ct'_{\text{pr}}}{2}\right)} = \\ &= \sqrt{\text{Var}\left(\frac{z_{\text{PV}}}{2} + \frac{ct_{\text{PV}}}{2} - \frac{ct'_{\text{pr}}}{2} - \frac{z'_{\text{pr}}}{2}\right)} = \\ &= \sqrt{4\frac{\sigma_{\text{BS}}^2}{4}} = \sigma_{\text{BS}}.\end{aligned}\tag{29}$$

References

- [1] Y. L. Dokshitzer, S. Troyan and V. A. Khoze, *Collective QCD Effects in the Structure of Final Multi - Hadron States. (In Russian)*, *Sov. J. Nucl. Phys.* **46** (1987) 712.
- [2] J. Bjorken, *Rapidity gaps and jets as a new physics signature in very high-energy hadron hadron collisions*, *Phys. Rev. D* **47** (1993) 101.
- [3] E. Feinberg and I. Pomerančuk, *High-energy inelastic diffraction phenomena*, *Nuovo Cim. Suppl.* **3** (1956) 652.
- [4] PARTICLE DATA GROUP collaboration, *Review of Particle Physics*, *PTEP* **2020** (2020) 083C01.
- [5] L. Evans and P. Bryant, *LHC machine*, *JINST* **3** (2008) S08001.
- [6] The ATLAS Collaboration, *Luminosity public results from LHC Run-2*. <https://twiki.cern.ch/twiki/bin/view/AtlasPublic/LuminosityPublicResultsRun2>.
- [7] P. Azzi et al., *Report from Working Group 1: Standard Model Physics at the HL-LHC and HE-LHC*, in *Report on the Physics at the HL-LHC, and Perspectives for the HE-LHC*, A. Dainese, M. Mangano, A. B. Meyer, A. Nisati, G. Salam and M. A. Vesterinen, eds., vol. 7, pp. 1–220, (12, 2019), [arXiv:1902.04070](https://arxiv.org/abs/1902.04070), DOI.
- [8] M. Albrow and A. Rostovtsev, *Searching for the Higgs at hadron colliders using the missing mass method*, [arXiv:hep-ph/0009336](https://arxiv.org/abs/hep-ph/0009336).
- [9] L. Adamczyk et al., *Technical Design Report for the ATLAS Forward Proton Detector*, Tech. Rep. CERN-LHCC-2015-009. ATLAS-TDR-024, CERN, May, 2015.
- [10] ATLAS Collaboration, *The ATLAS experiment at the CERN large hadron collider*, *Journal of Instrumentation* **3** (2008) S08003.
- [11] M. Albrow et al., *CMS-TOTEM Precision Proton Spectrometer*, Tech. Rep. CERN-LHCC-2014-021. TOTEM-TDR-003. CMS-TDR-13, CERN, Sep, 2014.

- [12] CMS collaboration, *The CMS Experiment at the CERN LHC*, *JINST* **3** (2008) S08004.
- [13] TOTEM collaboration, *Diamond Detectors for the TOTEM Timing Upgrade*, *JINST* **12** (2017) P03007 [[arXiv:1701.05227](#)].
- [14] ATLAS collaboration, *Exclusive Jet Production with Forward Proton Tagging*, Tech. Rep. ATL-PHYS-PUB-2015-003, CERN, Geneva, Feb, 2015.
- [15] L. Harland-Lang, V. Khoze, M. Ryskin and M. Tasevsky, *LHC Searches for Dark Matter in Compressed Mass Scenarios: Challenges in the Forward Proton Mode*, *JHEP* **04** (2019) 010 [[arXiv:1812.04886](#)].
- [16] M. Tasevsky, *Review of Central Exclusive Production of the Higgs Boson Beyond the Standard Model*, *Int. J. Mod. Phys. A* **29** (2014) 1446012 [[arXiv:1407.8332](#)].
- [17] R. Staszewski and J. Chwastowski, *Timing detectors for forward physics*, *Nucl. Instrum. Meth. A* **940** (2019) 45 [[arXiv:1903.03031](#)].
- [18] V. P. Gonçalves, D. E. Martins, M. S. Rangel and M. Tasevsky, *Top quark pair production in the exclusive processes at the LHC*, *Phys. Rev. D* **102** (2020) 074014 [[2007.04565](#)].
- [19] STAR collaboration, *Measurement of the central exclusive production of charged particle pairs in proton-proton collisions at $\sqrt{s} = 200$ GeV with the STAR detector at RHIC*, *JHEP* **07** (2020) 178 [[arXiv:2004.11078](#)].
- [20] ATLAS collaboration, *Technical Design Report: A High-Granularity Timing Detector for the ATLAS Phase-II Upgrade*, Tech. Rep. CERN-LHCC-2020-007. ATLAS-TDR-031, CERN, Geneva, Jun, 2020.
- [21] CMS collaboration, *Technical Propodal for a MIP Timing Detector in the CMS Experiment Phase 2 Upgrade*, Tech. Rep. CERN-LHCC-2017-027. LHCC-P-009, CERN, Geneva, Dec, 2017.
- [22] T. Sjöstrand, S. Mrenna and P. Skands, *A brief introduction to PYTHIA 8.1*, *Computer Physics Communications* **178** (2008) 852–867.